Journal of Applied Physics

RESEARCH ARTICLE | OCTOBER 02 2025

Characterizing the effects of temperature on the thermal vibration properties of individual nanowires

Ovidiu Cretu ; Han Zhang ; Koji Harano ; Koji Kimoto

J. Appl. Phys. 138, 134301 (2025)
https://doi.org/10.1063/5.0288200

Journal of Applied Physics METHOD pubs.aip.org/aip/jap

Characterizing the effects of temperature on the thermal vibration properties of individual nanowires

Cite as: J. Appl. Phys. **138**, 134301 (2025); doi: 10.1063/5.0288200
Submitted: 30 June 2025 · Accepted: 13 September 2025 ·
Published Online: 2 October 2025

View Online Export Citation CrossMark

Ovidiu Cretu,[1,a)] Han Zhang,[1] Koji Harano,[1,2] and Koji Kimoto[1]

AFFILIATIONS

[1]Center for Basic Research on Materials (CBRM), National Institute for Materials Science (NIMS), Namiki 1-1, Tsukuba, Ibaraki 305-0044, Japan
[2]Research Center for Autonomous Systems Materialogy (ASMat), Institute of Integrated Research, Institute of Science Tokyo, 4259 Nagatsuda-cho, Midori-ku, Yokohama, Kanagawa 226–8501, Japan

[a)]**Author to whom correspondence should be addressed:** cretu.ovidiu@nims.go.jp

ABSTRACT

We study the effects of temperature on the properties of thermal vibrations of individual LaB_6 single-crystal nanowires inside a transmission electron microscope using a method which combines high spatial resolution, high temporal resolution, and *in situ* temperature control. We find that the vibrations can be accurately modeled by classical formalisms, despite the small size of the resonator. We observe a vibration frequency decrease with temperature which enables us to measure the temperature coefficient of Young's modulus, finding a value of $\alpha_E \cong -9 \times 10^{-5}$ K^{-1} over the 300–700 K temperature range. We additionally introduce a method to precisely measure the vibration amplitude, which agrees well with values predicted by the Boltzmann equipartition theorem over the entire temperature range.

I. INTRODUCTION

The characterization of the vibration properties of nanometer-sized objects is important due to their applications as nanomechanical resonators.[1–3] Evaluating these properties is also critical in cases where vibration has detrimental effects on the function of these nanostructures, such as the loss of spatial coherence for electron sources.[4,5] Understanding temperature effects on these properties is important for devices operating as high-temperature resonators[6,7] or electron emitters, where temperature is used to lower the work function of the material and maintain a clean surface.[8] In addition, thermal activation is interesting for designing self-powered devices.[9]

Measuring vibration properties becomes increasingly challenging as the size of individual objects decreases and requires solutions such as coupling with optical cavities.[10] Electron microscopes offer excellent spatial resolution, but relatively poor temporal resolution when compared to the vibration frequency of nanostructures, which can easily extend beyond the MHz regime.[2] In order to overcome the temporal resolution limitation, previous studies have combined scanning electron microscopes (SEMs) and fast signal acquisition electronics in order to study the dynamics of individual vibrating objects.[11–15] In these cases, the measurements are limited by the nanometer-level spatial resolution of the microscope. An obvious solution is to use a transmission electron microscope (TEM), which is able to image nanomaterials with sub-angstrom resolution. We have recently introduced a method to separate and directly image thermal vibration modes in a TEM,[16] which showed excellent qualitative agreement between the measured and calculated mode shapes at room temperature.

In the present study, we extend our previous work by varying the temperature of the sample *in situ* using a heating holder and investigating the effects of temperature on the properties of thermal vibrations. The first part of the paper provides a detailed analysis in the time- and frequency domain of the signals which we collect during the experiment, which includes a comparison with simulated data. The second part analyzes the temperature dependency of the frequency variation with temperature, using mechanical vibration theory in order to model it and derive the temperature

coefficient of Young's modulus. The third part of the paper introduces a method to precisely measure the vibration amplitude, which is modeled by using the Boltzmann equipartition theorem. Finally, the main challenges and limitations are discussed in detail.

II. METHODS

The single-crystal LaB_6 nanowires used in this study were synthesized following a procedure described previously.[17] Briefly, BCl_3 gas and $LaCl_3$ powder were introduced in a quartz tube furnace and heated to 1150 °C; the nanowire growth occurred on a Pt-coated Si substrate, placed downstream from the location of the powder. An individual nanowire was deposited on the tip of a Ta needle using a nanomanipulator;[18] the nanowire was aligned to the axis of the needle. The Ta needle was then fixed on a 3 mm washer using Ag epoxy. The final assembly could be installed into a standard TEM sample holder. A low-magnification TEM image of the nanowire is displayed in Fig. S1 in the supplementary material, showing that the nanowire extends beyond the edge of the Ta needle by a distance of approximately 12 μm.

The experiments were performed using a TFS Titan^3 microscope, equipped with dual aberration-correctors and a monochromator. The microscope was operated at 80 kV in STEM (scanning) mode, with a convergence angle of 18 mrad, resulting in a probe size of less than 0.2 nm (FWHM). The probe current was set to approximately 100 pA. The sample was installed in a single-tilt MelBuild furnace-type heating holder, which allows for heating up to 600 °C. The temperature of the nanowire was varied between room temperature and 400 °C, with a soak time of more than 30 min after each temperature change.

An outline of the experimental setup is displayed in Fig. 1. The data were collected using a custom scanning and acquisition system,[16] composed of a scan controller implemented using a National Instruments (NI) PXIe-7862 field-programmable gate array (FPGA) based reconfigurable I/O module connected to the scan coils, together with a NI PXIe-5111 high-speed digitizer connected to a Gatan 806 high-angle annular dark-field (HAADF) detector. The data were acquired using NI LabVIEW and processed using ImageJ[19] and Gatan DigitalMicrograph. The experiment consisted of collecting the HAADF detector signal at high speed at each point, over the entire scanned area, resulting in a 3D data set. Data-cubes of 128 × 128 × 8192 voxels were collected at each temperature, using acquisition rates of 2 and 20 MHz at each scan point.

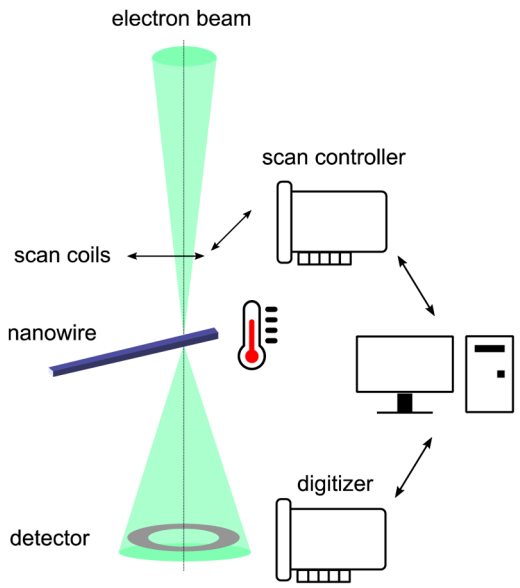

FIG. 1. Schematic description of the experiment.

In order to better understand the experimental results, the signals were simulated by generating square-wave functions and convoluting them with Gaussians, followed by Fourier analysis. Noise was also added to the calculated signals; however, it did not make any significant difference to the results. The calculations were performed using GNU Octave. The code used for the calculations can be found in the supplementary material.

III. RESULTS

A. Time-domain analysis

The signal collected by a STEM detector is usually constant at each scan position; in the case of a HAADF detector, it is approximately proportional to $Z^{1.7}t$, where Z is the average atomic number of the sample at that point and t is the thickness.[20] However, in our case, this signal is modulated by the thermal vibration of the nanowire. This is schematically illustrated in Fig. 2(a). Here, the nanowire vibrates between two extreme positions marked by orange and purple contours, its trajectory described by a sine function. When the electron beam is fixed in a position along this vibration path, the detector signal will be high (H) when the nanowire covers the beam and low (L) otherwise. Thus, the signal at the detector will be a square wave with the same period as the vibration of the nanowire. If the position of the beam is close to the outside contour [marked as "position 1" in Fig. 2(a)], the signal will be low for most of the vibration period, resulting in a low duty cycle. On the contrary, if the beam is fixed close to the inside contour [marked as "position 2" in Fig. 2(a)], it will be covered by the nanowire during most of the vibration period, resulting in a high duty cycle. It is important to note that the middle point of the vibration, marked by a black contour, is the only location where the signal has a 50% duty cycle.

This idealized explanation can be compared with the two experimental signals in Fig. 2(c), extracted from points "1" and "2" of the HAADF image in Fig. 2(b). While there is good agreement with respect to the duty cycle, the main difference with Fig. 2(a) is that the experimental signals appear rounded (softened). There are two main reasons for this, which will be discussed in detail in the later sections of the paper: the fact that the nanowire edge is not perfectly flat and the finite response time of the HAADF detector. A much closer match is obtained by comparing experimental data with the square-wave calculations in Fig. S2 in the supplementary material, which are described in detail below.

The signals in Fig. 2(c) can also be used in order to estimate the amount of noise present in our measurements. The bottom

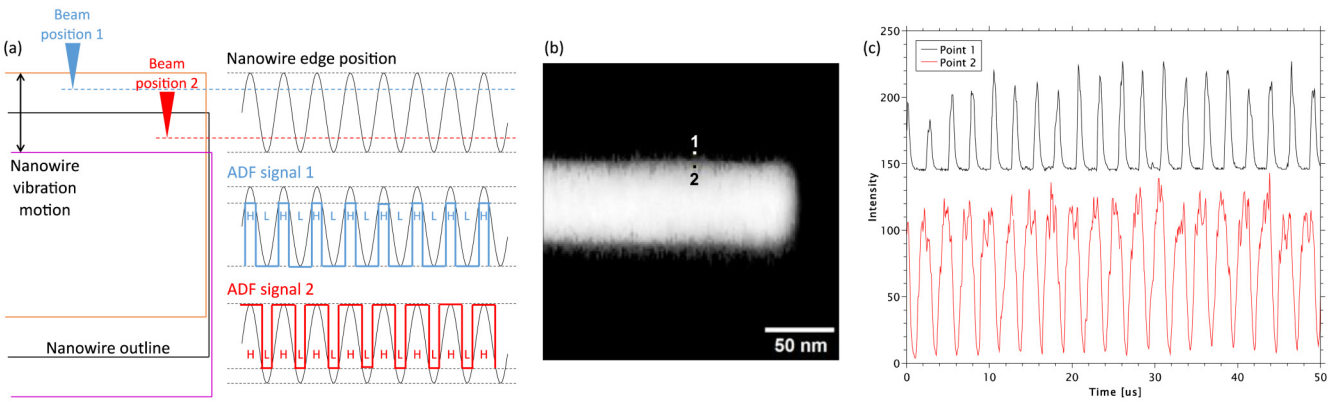

FIG. 2. Time-domain analysis. (a) Schematic illustration. (b) HAADF image of the tip of the nanowire. (c) Detector signal from points marked "1" and "2" in the image. The two signals have been manually offset for clarity.

part of the black curve (corresponding to point "1") shows the detector signal in the absence of the nanowire; the noise level is relatively low. The top part of the red curve (corresponding to point "2") shows the detector signal while the beam is covered by the nanowire; this curve appears noisy; however, this is the actual signal due to the overlap of the various vibration modes of the nanowire.

B. Frequency-domain analysis

Further insight can be gained by converting the time-domain data-cube into the frequency domain, which is done by applying a Fourier transform to the time-domain signal collected at each point. Figure 3(a) shows a HAADF image of the scanned area at the tip of the nanowire, while Fig. 3(d) shows the average FFT spectrum from the entire area. The two strongest peaks represent the 1st and 2nd harmonics of the first (fundamental) vibration mode of the nanowire. Mapping these two peaks over the entire scanned area produces the images in Figs. 3(b) and 3(c), respectively. The image in Fig. 3(b) represents the vibration profile of the nanowire, and we have previously shown that this type of analysis can be extended to the higher order vibration modes.[16]

It is interesting to note that the map in Fig. 3(c) shows a minimum. This is also visible in Fig. 3(e), which plots the intensities of the 1st and 2nd harmonics of the first vibration mode along the direction indicated by a white arrow. The explanation for this minimum can be found in the mathematical properties of the harmonics of square waves. A numerical simulation of this effect is shown in Fig. S2 in the supplementary material, which displays how the FFT spectrum of a square-wave changes as the duty cycle is increased, while all the other parameters are kept constant. The data show that, in the special case of a 50% duty cycle, all of the even harmonics are suppressed. This agrees well with our explanation in Fig. 2(a), where we pointed out that this corresponds to the middle point of the vibration of the nanowire. This can furthermore be interpreted as the position of the nanowire in the absence of any vibrations. The calculations are summarized in Fig. 3(f), which can be compared to the experimental data in Fig. 3(e). There is qualitative agreement between the two figures, with the biggest difference being that the peaks in Fig. 3(e) are asymmetric. This is due to the finite response time of the HAADF detector and will be discussed in detail below.

C. Temperature dependency of the vibration frequency

By performing the analysis in Fig. 3(d) for each temperature, we can determine the variation of the vibration frequency with temperature, which is plotted in Fig. 4(a). This phenomenon can be modeled using mechanical vibration theory. The fundamental vibration frequency of a beam which is clamped at one end is given by[21,22]

$$f = \frac{1}{2\pi}\frac{a^2}{\sqrt{m}}\sqrt{\frac{EI}{L^3}}, \tag{1}$$

where $a = 1.88$, m is the mass, E is Young's modulus, L is the length, and I is the cross-sectional area momentum of inertia $\left(\int y^2 dA\right)$. Considering that LaB_6 has cubic symmetry, we can assume isotropic thermal expansion,

$$I = I_0(1+\alpha\Delta T)^4;\ L = L_0(1+\alpha\Delta T);\ E = E_0(1+\alpha_E\Delta T), \tag{2}$$

where α is the thermal expansion coefficient and α_E is the thermal coefficient of Young's modulus. Combining Eqs. (1) and (2), we obtain

$$f = \frac{1}{2\pi}\frac{a^2}{\sqrt{m}}\sqrt{\frac{E_0 I_0}{L_0^3}}\sqrt{(1+\alpha\Delta T)(1+\alpha_E\Delta T)} \cong f_0\left(1+\frac{\alpha+\alpha_E}{2}\Delta T\right). \tag{3}$$

An identical expression can be obtained for each of the higher modes of vibration by changing the value of the parameter

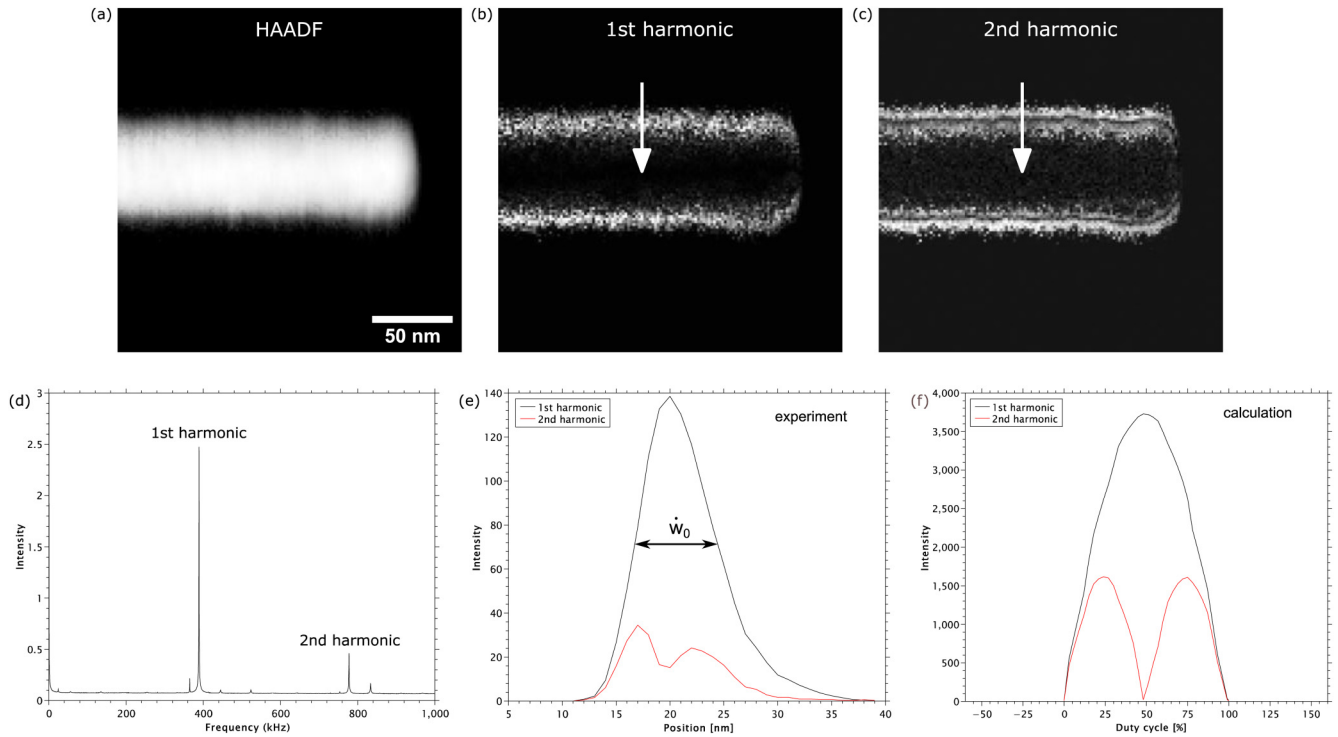

FIG. 3. Frequency-domain analysis. (a) HAADF image of the tip of the nanowire. (b) and (c) Maps of the 1st and 2nd harmonics of the first vibration mode in (d), respectively. (d) FFT spectrum extracted from the entire area in (a). (e) Averaged profiles along the direction marked by white arrows in (b) and (c). (f) Calculated intensities of the 1st and 2nd harmonics of a square wave, relative to the duty cycle.

a. The corresponding experimental data for the second and third modes are given in Figs. 4(b) and 4(c). Due to the higher frequencies, the data acquisition rate is higher, resulting in lower frequency resolution and, thus, higher measurement uncertainty for the second and third modes. The third mode compensates for the loss of frequency resolution by having a larger variation interval; however, it has the disadvantage of having a significantly reduced amplitude.

Using the experimental data in Fig. 4(a), we can determine the slope as $\alpha + \alpha_E \cong -8.28 \times 10^{-5}\ \mathrm{K}^{-1}$. Considering the thermal expansion coefficient as $\alpha \cong 7 \times 10^{-6}\ \mathrm{K}^{-1}$,[23] we finally get $\alpha_E \cong -9 \times 10^{-5}\ \mathrm{K}^{-1}$. Although we did not find any other

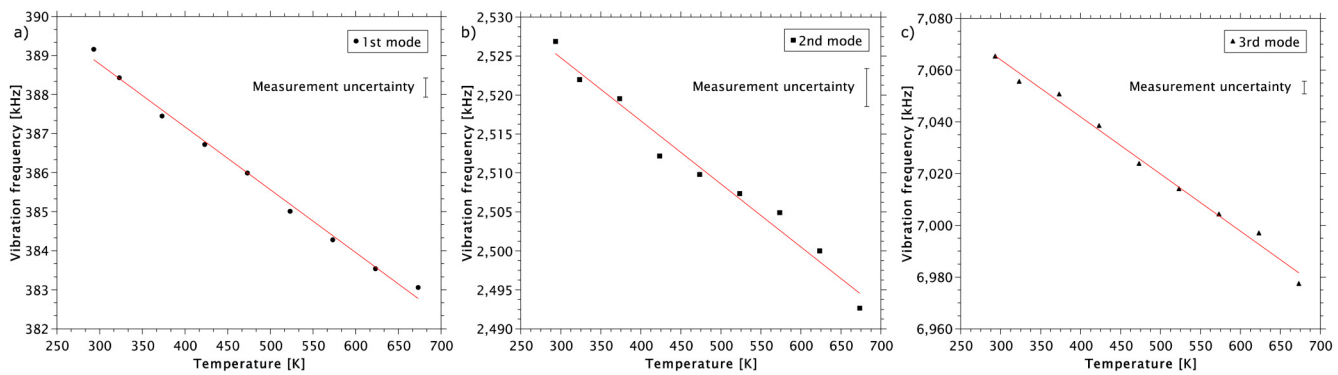

FIG. 4. Temperature dependency of the nanowire vibration frequency for the first three modes of vibration.

experimental data for this parameter, our value agrees well with the -1.5×10^{-4}[24] and -1.2×10^{-4} K^{-1}[25] values obtained by calculations, which confirms the validity of our method. It is important to mention that Eq. (3) does not require any prior knowledge or measurement of the nanowire's geometry or properties, which eliminates potential sources of error. Finally, it is interesting to note that the two thermal coefficients have opposite signs. Therefore, the decrease in frequency with temperature is due to the much larger temperature coefficient of Young's modulus. In the absence of this variation, due to thermal expansion alone, the frequency should display the opposite behavior and increase.

The absolute value of the frequency can be used to determine the exact length of the suspended part of the nanowire. Equation (1) can be re-written as

$$f = \frac{a^2}{2\pi L^2}\sqrt{\frac{EI}{\rho A}} \rightarrow L = a\sqrt{\frac{1}{2\pi f}\sqrt{\frac{EI}{\rho A}}}, \tag{4}$$

where ρ is the density and A is the area of the cross section of the nanowire. This expression is particularly convenient for cases where the cross section is not a simple geometric shape, such as the nanowire. An image of the cross section is shown in Fig. S3 in the supplementary material; these data were obtained by tomography, as described previously.[16,26] From the cross-sectional image, parameters A and I can be determined numerically; we obtain $A = 2.95 \times 10^3$ nm^2 and $I = 7.68 \times 10^5$ nm^4. Using these values, as well as $\rho = 4720$ kg/m^3 and $E = 467$ GPa,[27] we obtain $L = 15\,\mu$m. This length is significantly different from the $12\,\mu$m which can be measured in Fig. S1 in the supplementary material, implying that the suspended length of the nanowire extends approximately $3\,\mu$m inside the area covered by the Ta needle. Further proof that the part of the nanowire located close to the edge of the needle is vibrating is given in Fig. S4 in the supplementary material, which shows a high-resolution image of the nanowire lattice in that area. The profiles show that the lattice along the direction of the vibration ("Y") is much less resolved than the perpendicular direction ("X"), which should not be the case considering the cubic lattice of LaB_6 and is a result of blurring introduced by the vibration.

D. Temperature dependency of the vibration amplitude

The vibration amplitude can be obtained by fitting the profile of the 1st harmonic of the fundamental vibration mode in Fig. 3(e). We have found that a suitable expression for performing this fit is the "asymmetric peak" function implemented in Gatan's DigitalMicrograph software. This expression is defined as

$$g(x) = A\left[s\left(c_1\frac{\dot{w}}{4(x-x_0)^2+\dot{w}^2}\right) + (1-s)\left(\frac{c_2}{\dot{w}}e^{-c_3\left(\frac{x-x_0}{\dot{w}}\right)^2}\right)\right], \tag{5}$$

where $\dot{w} = x \cdot E + w$, $c_1 = 2/\pi$, $c_2 = \sqrt{4\ln(2)/\pi}$, $c_3 = 4\ln(2)$, A is the scale, x_0 is the position for $E = 0$, w is the FWHM for $E = 0$, E is the asymmetry factor, and s is the shape factor. All of the parameters in Eq. (5) are fitting parameters, except for x which is the independent variable. With respect to Fig. 3(e), x_0 is the location of the center of the curve (which indicates the equilibrium position of the nanowire), while $\dot{w}_0 = x_0 \cdot E + w$ represents the width (which is proportional to the vibration amplitude). The results of fitting the profile at each temperature are plotted in Fig. 5, by considering the vibration amplitude as $\dot{w}_0/2$.

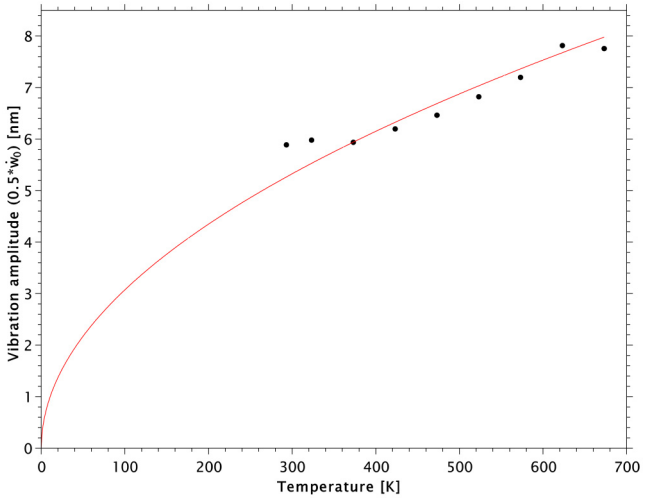

FIG. 5. Temperature dependency of the nanowire vibration amplitude.

The amplitude of the vibration can be modeled considering Boltzmann's equipartition theorem, which assigns each vibration mode an energy of $1/2\,kT$,[21]

$$z = \frac{2\sqrt{2}}{a^2}\sqrt{kT}\sqrt{\frac{L^3}{EI}}, \tag{6}$$

where k is Boltzmann's constant. Using the previously determined values for L and I, we obtain $z = 2.88 \times 10^{-10}\sqrt{T}$. This is in excellent agreement with the red curve in Fig. 5, which is obtained by fitting the experimental data $z = 3.07 \times 10^{-10}\sqrt{T}$.

It is interesting to note that, somewhat counterintuitively, this method cannot be used to obtain the amplitudes of the higher vibration modes. This is because the higher order modes are modulated by the fundamental mode. This modulation has the effect of extending the signal of the higher order vibrations to the entire area covered by the first mode. The opposite also holds; however, the effect should be less pronounced owing to the much smaller amplitudes of the higher order modes. Nevertheless, this could explain the slightly higher experimental value in the previous paragraph.

IV. DISCUSSION

There are two factors which complicate our measurements and analysis. The first and arguably the most important is the fact that the nanowire has an irregular, rounded cross section, as shown in Fig. S2 in the supplementary material. This distorts the time-domain signals in Fig. 2 and broadens the FFT intensity profiles in Fig. 3. Additionally, this complicates our modeling because

established expressions for simple geometrical shapes cannot be used. An even more straight-forward example of this problem is illustrated in Fig. S5 in the supplementary material, which shows averaged plots of the nanowire's width at different temperatures. There is no obvious broadening of the profiles, despite the increasing amplitude of the vibration.

Another important issue is the temporal resolution of the system, which is determined by the response time of the HAADF detector. The Gatan 806 detector has a scintillator/photomultiplier (PMT) design; the scintillator used is yttrium aluminum perovskite (YAP), which has a reported decay time constant of $\tau \sim 27$ ns,[28,29] resulting in a pulse width of $3\tau \sim 100$ ns. However, the PMT and downstream electronics broaden this pulse to ~400–500 ns.[30] This is likely due to design considerations since such a detector is mainly optimized for high gain and low noise. This becomes an issue when collecting square-wave signals with a very high dwell-time since, as illustrated in Fig. 2(a), the time when the signal is low can be much shorter than the $\sim 2.5\,\mu$s vibration period of the nanowire, preventing the detector signal from returning to its initial level. Since these high dwell-time signals are located toward the interior of the nanowire, this could explain why the peaks in Fig. 3(e) show an asymmetry in that region. While the current setup is limited in terms of time resolution to ~10 MHz, the latest generation of fast scintillator detectors have shown response times down to ~1 ns,[31] which would allow vibration measurements into the GHz regime and extend the methods shown here to a wide variety of nanoresonators.

Lastly, the agreement between the measured and calculated vibration amplitudes allows us to infer that there is no difference between the actual temperature of the nanowire and the value set using our heating holder. This fits well with estimates according to which the temperature of ceramics should increase by less than 0.1 K when using a 100 pA electron probe.[32] Another argument comes from the fact that the irradiated region of the nanowire shown in Figs. 2(b) and 3(a) is ~150 nm in length, which represents ~1% of the total volume of the nanowire, considering the 15 μm length estimated earlier. Therefore, we can confidently state that heating by the electron beam is negligible in our experiments.

V. CONCLUSIONS

In conclusion, we have combined the well-known spatial resolution of the TEM with the high temporal resolution of our custom acquisition system and with temperature control in order to gain insight into how temperature influences the thermal vibration properties of individual nanowires. Within the constraints of our experiments, the nanowire vibration can be accurately modeled by classical formalisms, such as mechanical vibration theory and Boltzmann's equipartition theory, despite the small size. We have taken advantage of this in order to measure material properties which would otherwise be difficult to determine, such as the temperature coefficient of Young's modulus.

SUPPLEMENTARY MATERIAL

See the supplementary material for a low-magnification image of the nanowire (Fig. S1), square-wave signals and corresponding FFTs (Fig. S2), nanowire cross section (Fig. S3), nanowire high-resolution data near the end of the Ta needle (Fig. S4), and HAADF profiles of the nanowire at various temperatures (Fig. S5).

ACKNOWLEDGMENTS

This work was supported by JSPS KAKENHI Grant Nos. JP24K08253 (O.C.), JP23H04874 (K.H.), and JP22H05145 (K.K.).

AUTHOR DECLARATIONS

Conflict of Interest

The authors have no conflicts to disclose.

Author Contributions

Ovidiu Cretu: Conceptualization (lead); Formal analysis (lead); Funding acquisition (equal); Investigation (lead); Methodology (lead); Writing – original draft (lead); Writing – review & editing (lead). **Han Zhang:** Conceptualization (supporting); Investigation (supporting); Methodology (supporting); Validation (equal); Writing – review & editing (supporting). **Koji Harano:** Funding acquisition (equal); Resources (equal); Validation (equal); Writing – review & editing (supporting). **Koji Kimoto:** Funding acquisition (equal); Resources (equal); Supervision (lead); Validation (equal); Writing – review & editing (supporting).

DATA AVAILABILITY

The data that support the findings of this study are available from the corresponding author upon reasonable request.

REFERENCES

[1]B. Xu, P. Zhang, J. Zhu, Z. Liu, A. Eichler, X.-Q. Zheng, J. Lee, A. Dash, S. More, S. Wu, Y. Wang, H. Jia, A. Naik, A. Bachtold, R. Yang, P. X.-L. Feng, and Z. Wang, ACS Nano **16**, 15545 (2022).
[2]A. Bachtold, J. Moser, and M. I. Dykman, Rev. Mod. Phys. **94**, 045005 (2022).
[3]N. Ghaemi, A. Nikoobin, and M. R. Ashory, Adv. Electron. Mater. **8**, 2200229 (2022).
[4]N. de Jonge, J. Appl. Phys. **95**, 673 (2004).
[5]H. Zhang, Y. Jimbo, A. Niwata, A. Ikeda, A. Yasuhara, O. Cretu, K. Kimoto, T. Kasaya, H. T. Miyazaki, N. Tsujii, H. Wang, Y. Yamauchi, D. Fujita, S. Kitamura, and H. Manabe, Nat. Nanotechnol. **17**, 21 (2022).
[6]F. Ye, J. Lee, and P. X.-L. Feng, in *2018 IEEE International Electron Devices Meeting (IEDM)* (IEEE, 2018).
[7]L. Sang, H. Sun, X. Yang, T. Li, B. Shen, and M. Liao, in *2020 IEEE International Electron Devices Meeting (IEDM)* (IEEE, 2020).
[8]S. Yamamoto, Rep. Prog. Phys. **69**, 181 (2006).
[9]Y. Qiao, A. Elhady, M. Arabi, E. Abdel-Rahman, and W. Zhang, Microsyst. Nanoeng. **10**, 90 (2024).
[10]A. W. Barnard, M. Zhang, G. S. Wiederhecker, M. Lipson, and P. L. McEuen, Nature **566**, 89 (2019).
[11]P. Vincent, S. Perisanu, A. Ayari, M. Choueib, V. Gouttenoire, M. Bechelany, A. Brioude, D. Cornu, and S. T. Purcell, Phys. Rev. B **76**, 085435 (2007).
[12]H. Wang, J. C. Fenton, O. Chiatti, and P. A. Warburton, Rev. Sci. Instrum. **84**, 075002 (2013).

[13]I. Tsioutsios, A. Tavernarakis, J. Osmond, P. Verlot, and A. Bachtold, Nano Lett. **17**, 1748 (2017).
[14]L. M. Vogl, P. Schweizer, P. Denninger, G. Richter, and E. Spiecker, ACS Nano **16**, 18110 (2022).
[15]C. Chardin, S. Pairis, S. Douillet, M. Hocevar, J. Claudon, J.-P. Poizat, L. Bellon, and P. Verlot, Nano Lett. **25**, 4774 (2025).
[16]O. Cretu, H. Zhang, and K. Kimoto, Nano Lett. **22**, 10034 (2022).
[17]H. Zhang, J. Tang, Q. Zhang, G. Zhao, G. Yang, J. Zhang, O. Zhou, and L-C Qin, Adv. Mater. **18**, 87 (2006).
[18]H. Zhang, J. Tang, J. Yuan, Y. Yamauchi, T. T. Suzuki, N. Shinya, K. Nakajima, and L.-C. Qin, Nat. Nanotechnol. **11**, 273 (2016).
[19]J. Schindelin, I. Arganda-Carreras, E. Frise, V. Kaynig, M. Longair, T. Pietzsch, S. Preibisch, C. Rueden, S. Saalfeld, B. Schmid, J.-Y. Tinevez, D. J. White, V. Hartenstein, K. Eliceiri, P. Tomancak, and A. Cardona, Nat. Methods **9**, 676 (2012).
[20]S. Yamashita, J. Kikkawa, K. Yanagisawa, T. Nagai, K. Ishizuka, and K. Kimoto, Sci. Rep. **8**, 12325 (2018).
[21]H.-J. Butt and M. Jaschke, Nanotechnology **6**, 1 (1995).
[22]S. S. Rao, *Mechanical Vibrations* (Prentice Hall, Upper Saddle River, NJ, 2011).
[23]C.-H. Chen, T. Aizawa, N. Iyi, A. Sato, and S. Otani, J. Alloys Compd. **366**, L6–L8 (2004).
[24]X. Guo-Liang, C. Jing-Dong, X. Yao-Zheng, L. Xue-Feng, L. Yu-Fang, and Z. Xian-Zhou, Chin. Phys. Lett. **26**, 056201 (2009).
[25]D. Zakarian and A. Khachatrian, JOJ Mater. Sci. **2**, 555580 (2017).
[26]R. Huber, G. Haberfehlner, M. Holler, G. Kothleitner, and K. Bredies, Nanoscale **11**, 5617 (2019).
[27]H. Zhang, J. Tang, L. Zhang, B. An, and L.-C. Qin, Appl. Phys. Lett. **92**, 173121 (2008).
[28]S. Kishimoto and T. Yamamoto, Nucl. Instrum. Methods Phys. Res. A **508**, 425 (2003).
[29]M. Moszyński, M. Kapusta, D. Wolski, W. Klamra, and B. Cederwall, Nucl. Instrum. Methods Phys. Res. A **404**, 157 (1998).
[30]T. Mullarkey, M. Geever, J. J. P. Peters, I. Griffiths, P. D. Nellist, and L. Jones, Microsc. Microanal. **29**, 1402 (2023).
[31]Exosens ScintiFast Technology, see https://www.exosens.com/products/scintifasttm-technology for details about the scintillator pulse shape (accessed 27 May 2025).
[32]D. B. Williams and C. B. Carter, *Transmission Electron Microscopy a Textbook for Materials Science* (Springer US, Boston, MA, 2009).